RSC Sustainability

ROYAL SOCIETY OF CHEMISTRY

TUTORIAL REVIEW

View Article Online
View Journal | View Issue

Cite this: *RSC Sustainability*, 2026, **4**, 2099

Optical detection of hydrogen gas using organic dyes and metal-based activators: a review

Mark Potter, [a] Marcus W. Drover *[b] and Simon Rondeau-Gagné *[a]

The adoption of hydrogen gas ($H_{2(g)}$) as a carbon-free energy source requires reliable, sensitive, and accessible detection technologies for use across various environments. Optical $H_{2(g)}$ sensors based on organic dyes offer an attractive alternative to traditional sensors by providing selective and sensitive visual readouts, with low power consumption, and compatibility with simple and miniature devices. However, the relative inertness of $H_{2(g)}$ under ambient conditions necessitates indirect detection relying on $H_{2(g)}$ activation coupled with optical response. This review provides a comprehensive and mechanistic overview of fluorescence- and colorimetric-based $H_{2(g)}$ sensors that employ organic dyes in combination with metal-based activating agents. We discuss how $H_{2(g)}$ activation is dominated through two strategies: (1) surface mediated activation at noble metal surfaces with supported catalysts and nanoparticles; and (2) organometallic mediated activation. Emphasis is placed on sensor performance and usability with respect to activation pathway, dye selection, and sensor architecture. By critically comparing reported sensing performances, we identify key design principles that directly influence $H_{2(g)}$ sensing ability across different dye-based sensors including dye, activator, and architecture selection. We also highlight the need for benchmarked parameters which currently limits cross-study comparison and rational design. Finally, we outline future opportunities for sustainable optical dye-based $H_{2(g)}$ detection related to improving currently available systems. Altogether, this review aims to provide a guide for the development of next-generation optical $H_{2(g)}$ sensors that support the safe and sustainable integration of $H_{2(g)}$-based technologies into society.

Received 4th March 2026
Accepted 1st April 2026

DOI: 10.1039/d6su00135a

rsc.li/rscsus

[a]*Department of Chemistry and Biochemistry, University of Windsor, 401 Sunset Ave., Windsor, Ontario, N9B 3P4, Canada. E-mail: srondeau@uwindsor.ca*

[b]*Department of Chemistry, Western University, 1151 Richmond Street, London, ON, N8K 3G6, Canada. E-mail: marcus.drover@uwo.ca*

Mark Potter

Mark Potter received his BSc in Biochemistry and Biomedical Sciences (Thesis) from the University of Windsor, where he is currently completing his PhD in Chemistry and Biochemistry under the co-supervision of Prof. Simon Rondeau-Gagné and Prof. Bulent Mutus, supported by an NSERC PGS-D scholarship. His doctoral research focuses on the design and development of advanced dye-based fluorescent sensors for emerging environmentally relevant analytes, with additional contributions in the synthesis and characterization of functional polymer systems.

Marcus W. Drover

Marcus W. Drover earned his PhD at the University of British Columbia (2016) with Laurel L. Schafer and Jennifer A. Love, then moved to Caltech as a Banting/Resnick Sustainability Postdoctoral Fellow with Jonas C. Peters (2017–2019). He launched his independent career at the University of Windsor in 2019 and joined Western University in 2023, receiving tenure to Associate Professor in 2025. His work explores organometallic and main-group chemistry for sustainable solutions. Drover has co-authored >80 articles and serves on multiple editorial and early-career advisory boards in leading chemistry journals such as Organometallics and JACS Au.

Sustainability spotlight

The transition to a hydrogen-based energy economy requires reliable and intrinsically safe sensing technologies to ensure the secure deployment of hydrogen infrastructure. This review highlights advances in dye-based optical hydrogen sensors, which offer spark-free operation, remote monitoring capability, and compatibility with distributed sensing networks. By examining sensing platforms through a sustainability lens, including reliance on precious metals, material lifecycle considerations, and energy-efficient detection strategies, this work identifies pathways toward greener sensor design aligned with the principles of green chemistry. Improved hydrogen detection directly supports the safe integration of renewable hydrogen systems and global decarbonization efforts. These advances align with the United Nations Sustainable Development Goals, particularly SDG 7 (Affordable and Clean Energy), SDG 9 (Industry, Innovation and Infrastructure), and SDG 13 (Climate Action).

1 Introduction

Carbon dioxide (CO_2) emissions reached 33.3 metric gigatons in 2019, a growing rate that has contributed to Earth's ever-rising temperature.[1] Energy-related sectors are the largest contributors to CO_2 emissions due to their reliance on fossil fuels. Therefore, there is currently a global transition away from traditional fossil fuels towards low-carbon and/or carbon-neutral energy sources.[2,3] Among these alternatives, hydrogen gas ($H_{2(g)}$) has emerged as a promising energy carrier due to its carbon-free combustion and high gravimetric energy of $\sim$120 kJ g^{-1}, the highest of all known substances and nearly three times as high as conventional gasoline at $\sim$44 kJ g^{-1}.[4] Despite these advantages, the widespread adoption of $H_{2(g)}$ as a fuel source remains hindered by significant safety and infrastructure challenges.[5] $H_{2(g)}$ is colourless, tasteless, and odorless, making it undetectable by human senses.[6] In addition, $H_{2(g)}$ has an extremely high diffusion speed in air, readily permeates containment due to its small molecular size, and has a broad flammable concentration range of 4–75% (v/v).[4] These properties make $H_{2(g)}$ particularly susceptible to undetected leakage and explosion risk, highlighting the need for rapid, sensitive, and reliable detection technologies to prevent economic loss and enable its safe, large-scale adoption.[7]

The global demand for $H_{2(g)}$ has grown steadily and is expected to continue increasing as $H_{2(g)}$ production, transport infrastructure, industrial, and end-use applications continue to expand.[8,9] As $H_{2(g)}$ use across industrial and energy sectors increases, the development of robust $H_{2(g)}$ sensing technologies is crucial for ensuring the safety of industrial workers and end users. As such, a considerable amount of research has been directed toward the development of $H_{2(g)}$ sensors that meet performance requirements for practical use.[10] An effective $H_{2(g)}$ sensor should operate across relevant concentration ranges (typically 0.1 to 10% v/v) and under relevant temperatures (−30 to 80 °C), have rapid response times ($\sim$1 s), maintain an accuracy of $\pm$ 5%, and demonstrate long-term stability over operational lifetime approaching 10 years.[11] Additional attributes include resistance to interference from other organic molecules, low power consumption, compact size, explosion resistance, low cost, and ease of use.[12] To address these requirements, a wide range of $H_{2(g)}$ sensing technologies have been developed, including electrochemical sensors,[13,14] thermal conductivity detectors,[15–17] catalytic sensors,[18–20] metal oxide semiconductors,[21–23] mechanical sensors,[24] and even those relying on more standard analytical techniques such as gas chromatography and mass spectrometry.[12] While many of these approaches offer high sensitivity and reliability, they often require elevated operating temperatures, complex or bulky instrumentation, are cross reactive, or require large power inputs, potentially limiting their use in real-world applications.[12] Most commercially available $H_{2(g)}$ sensors are electrochemical in nature due to their high sensitivity and fast response times, however the calibration needs, temperature dependence, and low long term stability limits their use.[12,25]

Optical chemical sensors enable remote readout, simplified device structure, and spark-free operation, providing a compelling alternative.[12] These sensors convert chemical information into an optical signal due to interactions between the sensing material and analyte.[26] Among optical sensing approaches, fluorescence-based sensors are particularly attractive due to their high sensitivity and selectivity, compatibility with low-cost and miniature devices, and potential integration into wearable platforms.[27] Despite these advantages, optical-based detection of $H_{2(g)}$ presents several fundamental challenges that distinguish it from analogues that sense other gaseous analytes. $H_{2(g)}$ cannot be detected directly using conventional UV-visible absorption or fluorescence spectroscopy.[28] Moreover, $H_{2(g)}$ is a highly stable nonpolar diatomic molecule and interacts only weakly with organic dyes, rendering the use of common chemical sensing strategies based on intermolecular reactions or interactions ineffective. In addition to these spectroscopic limitations, the covalent H–H bond is highly stable, with a bond dissociation energy (BDE) of $\sim$436 kJ mol^{-1} (104 kcal mol^{-1}), making direct chemical reactions with unsaturated organic

Simon Rondeau-Gagné

Simon Rondeau-Gagné earned his PhD in Chemistry from Université Laval in 2014 with Prof. Jean-François Morin, followed by a FRQNT-funded postdoctoral fellowship with Zhenan Bao at Stanford University. He joined the University of Windsor in 2016, was promoted to Associate Professor in 2021, and has held a University of Windsor Research Chair since 2023. His research focus on advanced electronic polymers and related sensing technologies, with a focus on supramolecular strategies to create stretchable, self-healing materials for next-generation electronic and biointegrated devices.

functional groups, for example, unfavourable.[29] To make $H_{2(g)}$ reactive towards these substrates, dissociation and activation of $H_{2(g)}$ into a more reactive form is necessary.[30] Most commonly, this is achieved through the use of metal-containing additives, elevated temperature, or the use of electron rich co-sensors, such as dye molecules.[31–33] To date, most $H_{2(g)}$ sensors incorporate a metal-based catalyst or other activating agent(s). Noble metals and some organometallic complexes can bind $H_{2(g)}$ and disrupt the H–H bond to form metal–dihydrogen complexes $\{M^n\text{–}(H_2)\}$ or metal hydride species $\{M^{n+2}\text{–}(H)_2\}$.[34–37] These activated hydrogen intermediates can participate in subsequent chemistry, such as the hydrogenation of organic dyes which directly alters its electronic structure and photophysical properties, leading to a detectable optical change.[38] All reported dye-based $H_{2(g)}$ sensors rely on this hybrid detection strategy, in which $H_{2(g)}$ is chemically activated before an optical response is generated *via* transfer of the activated $H_{2(g)}$ to an organic dye, as will be discussed here. Hybrid systems that combine organic dyes with hydrogen-activating components therefore dominate design strategy for optical- and fluorescence-based $H_{2(g)}$ sensing across a variety of sensor format applications.

In addition to these hybrid sensing strategies, a range of optical $H_{2(g)}$ sensors have been developed that do not directly rely on organic dyes or fluorophores for signal generation. These dye-free systems typically exploit changes in optical properties of metal or metal-oxide materials such as palladium (Pd), magnesium (Mg), yttrium (Y), or tungsten oxide (WO_3) after $H_{2(g)}$ interaction which leads to changes in reflectance, transmittance, refractive index, or visible colour.[39–42] These sensors are commonly fabricated as thin films, multilayer devices, or nanostructured materials and frequently incorporate additional metals or functional layers to enhance performance.[43–54] While such systems fall outside of the scope of this review, they provide important context for evaluating dye-based systems, particularly with respect to signal generation and performance. Compared to these dye-free systems, dye-containing hybrid optical sensors offer advantages in signal amplification, tunability, and compatibility with low-cost, potentially portable detection platforms, making them attractive alternatives for $H_{2(g)}$ sensing applications.

This review provides an overview of optical- and fluorescence-based $H_{2(g)}$ detection methods that use organic dyes and other co-additive(s). We will focus on the underlying chemical and mechanistic principles that enable $H_{2(g)}$ sensing by clarifying how $H_{2(g)}$ activation, signal transduction, and dye–catalyst interactions result in operational sensors. This review aims to provide a conceptual framework that guides the rational design of next-generation organic dye-based $H_{2(g)}$ sensors and provides a cohesive discussion of known dye-based $H_{2(g)}$ sensors currently described in the literature.

2 Design principles governing dye-based optical hydrogen gas sensors

The performance of dye-based optical $H_{2(g)}$ sensors is governed by the relationship between the dye molecule, the $H_{2(g)}$ activating agent, and the material architecture. Across all systems reviewed below, the dye defines how information is reported, while the activator determines how efficiently $H_{2(g)}$ is converted into a chemically reactive species capable of interacting with the dye. Effective sensor design requires optimization of the dye, activating agent and the architecture of the sensor, as the sensing parameters of optical-based $H_{2(g)}$ sensors are drastic altered depending on these components. The key design characteristics and parameters which will be discussed in detail below are outlined in Fig. 1.

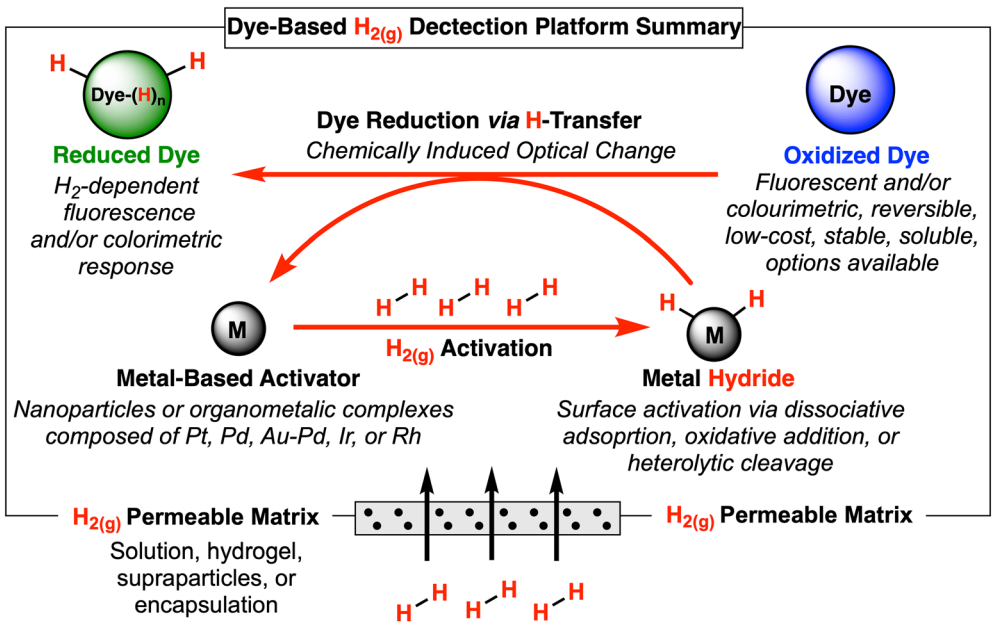

Fig. 1 Summary of key components and design considerations for optical dye-based $H_{2(g)}$ sensors.

2.1. Dye considerations

The dye is the signal generating component and thus dictates the sensitivity, readout modality, and practical useability of the sensor. Dyes employed in $H_{2(g)}$ sensing must undergo a chemically induced optical change, most commonly *via* reduction or hydrogenation, upon reaction with activated $H_{2(g)}$ species. Redox active dyes are particularly effective, as their optical response can be directly coupled to $H_{2(g)}$ activation.

Fluorescent dyes generally provide high sensitivity and lower detection limits than colorimetric (visual) sensors due to intrinsic signal amplification and reduced background interference.[55] This advantage is evident from sensors discussed below which utilize fluorescent dyes for quantitative $H_{2(g)}$ detection. However, fluorescence detection requires an external excitation source, optical filters, and a detector which must be considered during final device fabrication.[56] Either way, fluorescence-based sensors are desirable for applications that require highly accurate $H_{2(g)}$ detection demonstrated by their low detection limits. In contrast, colorimetric dyes, in some cases, enable instrument-free detection and straightforward visual interpretation but typically offer lower sensitivity and are often restricted to qualitative or semi-quantitative analysis.[57] An important design insight emerging from the studies reviewed is that dyes exhibiting both absorbance and fluorescence changes provide the greatest versatility, enabling naked-eye and quantitative detection.

Reversibility is another key parameter to consider, as reversible dyes enable continuous monitoring and cycling, while irreversible dyes are often better suited for one-time exposure sensing. The systems discussed and reviewed in the next pages demonstrate that reversibility is dictated not only by dye but also activator choice and $H_{2(g)}$ exposure, showing system-level design considerations, discussed below.

Beyond optical performance, practical constraints strongly influence dye selection. Solubility, compatibility with different matrices, photostability, shelf life, cost, and commercial availability all become defining factors for real-world sensors. Importantly, dyes must possess functional groups which can be reduced or hydrogenated, in turn altering the optical output for a detectable response. This point also highlights the necessity of an effective $H_{2(g)}$ activating agent when designing a dye-based optical $H_{2(g)}$ sensor.

2.2. Hydrogen gas activator considerations

Since $H_{2(g)}$ is relatively unreactive toward organic dyes under ambient conditions, all dye-based optical $H_{2(g)}$ sensors rely on metal-containing activating agents to generate reactive hydrogen species. The choice of activator not only determines how $H_{2(g)}$ is activated but also impacts the sensor's performance. Two dominating strategies emerge from the literature which are (i) surface mediated activation *via* Pd/C composite (Section 3.1.1.), or noble metal nanoparticles (NPs, (Sections 3.1.2. and 3.1.3.)) and (ii) organometallic complex activation at discrete metal centers (Section 3.2.).

Surface-mediated activators, most commonly noble-metal nanoparticles or supported catalysts, dissociate $H_{2(g)}$ at the metal surface to generate surface bound reactive hydrogen species.[58] These systems are well suited for solid-state sensor architectures, including films, composites, and supraparticles (SPs). Although with SP, humidity is still required for reduction of dyes to take place. Activator performance in these systems is governed by identity, particle size, dispersion, and accessibility.[59] The literature shows that small Pt-based NP maximize $H_{2(g)}$ activation rates, whereas Pd-based systems may suffer from slow activation rates due to $H_{2(g)}$ absorption into the bulk phase.[60] These factors directly influence response time, sensitivity, and reproducibility.

In contrast, organometallic complexes activate $H_{2(g)}$ most commonly through oxidative addition or heterolytic cleavage, forming metal-hydride intermediates.[36,37] These systems favour dyes capable of direct hydride acceptance from the metal center. Based on the literature reviewed in the next sections, the organometallic complex-based $H_{2(g)}$ sensors have primarily been investigated in solution or within hydrogel matrices, which impact available design approaches. As the dyes used are typically water soluble, the organometallic complex used must also have sufficient aqueous stability and solubility. From a practical standpoint, the use of organometallic complexes can reduce the overall noble metal load relative to surface mediated systems, although this is offset by increased synthetic complexity. As such, cost, synthetic simplicity, and long-term stability are important considerations for developing real-world sensors.

While these organometallic complexes can act catalytically, the overall sensor may respond stoichiometrically if dye reduction/hydrogenation is irreversible as is the case with many of the dyes reviewed. As a result, sensor performance, reversibility, and useability are dictated by the combined behaviour of the dye-$H_{2(g)}$ activator combination, rather than either component in isolation.

2.3. Architecture considerations

Beyond dye and $H_{2(g)}$ activator selection, the physical architecture of the dye-based optical $H_{2(g)}$ sensor plays a crucial role in determining performance, usability, and application. The reviewed literature below demonstrates that sensor behaviour is strongly influenced by whether the sensing components are in solution, embedded in hydrogel matrices, SP assemblies, or encapsulated. Each architecture imposes constraints on $H_{2(g)}$ transport, dye mobility, response kinetics, and stability. Solution-based sensors provide the highest degree of molecular freedom, enabling rapid $H_{2(g)}$ activation and efficient dye–activator interactions leading to fast response times. This architecture offers rapid response rates but is sensitive to evaporation and is best suited for laboratory-based sensing. Although, with specialized equipment, these sensors may be field deployable. Hydrogels retain advantages of solution-based sensing while enabling physical confinement and handling.[61] By imbedding dyes and metal activators within a hydrated polymer network, hydrogels retain water to maintain aqueous-dependent reactions and molecular mobility, while allowing fabrication of physical sensors. Parameters such as polymer

identity, crosslinking density, and water content directly influence $H_{2(g)}$ diffusion, response time, and dye mobility.[62] Articles reviewed demonstrate that hydrogels can preserve $H_{2(g)}$ sensitivity while enabling deployment for more different applications.

SPs represent a highly integrated, multicomponent approach in which dyes, catalysts, and structural components are co-localized within a mesoporous framework.[59] This enables precise control over catalyst dispersion, pore size, water content, and dye loading, allowing tuning of response time, sensitivity, and optical contrast. However, SP synthesis can be complex, requiring careful optimization of these multiple components which all effect sensor performance. SPs offer exceptional tunability and strong optical response, but their performance is sensitive to small changes in composition, highlighting trade-off between structural control and complexity.

Encapsulation can also provide an effective process for transitioning to the solid-state, preventing evaporation while maintaining $H_{2(g)}$ permeability and sensing performance. Additionally, encapsulation of sensing components within polymers can enable solvent-free sensor operation.[63] In both cases, direct integration into practical devices can be achieved. However, encapsulant material and thickness are important considerations, as they will determine gas permeability, leading to diffusion dependent responses which may reduce response time. On the other hand, encapsulation can improve mechanical stability and scalability providing additional useability.

Collectively, these architectures demonstrate that sensor performance is dictated by not only dye and $H_{2(g)}$ activator chemistry, but also by how these components interact in each design. Selecting an appropriate architecture therefore requires balancing sensitivity, response time, durability, scalability, and consideration of the intended application.

With these fundamental design considerations in mind, we now examine how these principles have been implemented across reported optical $H_{2(g)}$ sensors. The following sections critically review dye-based optical sensors, organized by $H_{2(g)}$ activation strategies with an emphasis on how variations in dye, activator, and sensor design translates into measurable differences in performance such as selectivity, response time, reversibility, and usability. This review provides a direct comparison between systems to provide rational design considerations to inform future optical dye-based $H_{2(g)}$ sensor design.

3 Dye–catalyst hybrid optical hydrogen gas detection

The chemical constraints associated with direct $H_{2(g)}$ detection necessitate the use of activating agents for optical sensing using organic dyes. As a result, most reported dye-based optical hydrogen sensors rely on multicomponent or hybrid systems in which $H_{2(g)}$ activation and signal generation are performed by distinct chemical components, as is described here. Within this framework, the organic dye functions as the optical signal transducer, while the metal-containing activator functions as the primary recognition element. Despite wide variation in sensor design, materials, and intended applications, the underlying operating principle of these systems are remarkably consistent. $H_{2(g)}$ is first activated at a metal center or surface before chemical modification of the incorporated dye occurs, altering its optical properties and producing a detectable response. The observed signal therefore reflects the chemical consequences of $H_{2(g)}$ activation rather than direct interaction of $H_{2(g)}$ and the organic dye molecule.

Reported dye-based optical $H_{2(g)}$ sensors can be broadly categorized according to how $H_{2(g)}$ activation is achieved because the transduction pathway remains consistent between all systems. The next sections are organized based on the hydrogen activating agent employed, with emphasis placed on how each class of activator is different, enables hydrogen activation, and optical transduction. While these approaches differ in practical performance, materials, and application, they all rely on the same fundamental relationship between $H_{2(g)}$ activation and dye-based signal generation. The following sections discuss dye-based optical $H_{2(g)}$ sensors that utilize distinct classes of $H_{2(g)}$ activating agents based on noble-metals either in the form of supported composites, NPs, or SPs architectures, which utilize surface mediated activation of $H_{2(g)}$, as well as organometallic complexes, which undergo metal center mediated activation of $H_{2(g)}$.

3.1. Noble-metal surface activation of hydrogen gas for dye-based optical sensing

Noble-metal surface activation represents the most widely employed strategy for $H_{2(g)}$ activation in dye-based $H_{2(g)}$ sensors. In these systems, $H_{2(g)}$ is adsorbed at the surface of the noble metals, most commonly Pd or Pt, generating reactive surface bound hydrogen species that participate in chemical transformations of associated dyes.[64] The surface-mediated activation enables $H_{2(g)}$ sensing under ambient conditions and is compatible with a wide range of sensor designs including supported metal composites, NPs, and SPs. Although these sensor designs range in complexity and application, they share a common mechanistic foundation of $H_{2(g)}$ activation at metal surface followed by an optical response by dye alteration. As such, differences in sensor performance generally arise from sensor design and dye selection rather than fundamentally different $H_{2(g)}$ activation pathways/mechanisms.

3.1.1. Pd/C nanocomposites. Among noble-metal catalysts capable of $H_{2(g)}$ activation, palladium-on-carbon (Pd/C) nanocomposites represent an established platform for $H_{2(g)}$ activation across a range of applications. In these materials, Pd is dispersed on high-surface-area carbon support, which serves both to stabilize the metal and to maximize accessibility to catalytic sites. Pd readily activates $H_{2(g)}$ under ambient conditions through dissociative adsorption, generating surface bound reactive metal-hydride species in the form of Pd–H. The activated hydrogen can subsequently participate in hydrogenation reactions and have been widely used in $H_{2(g)}$ getter technologies, and more recently, in optical $H_{2(g)}$ sensing

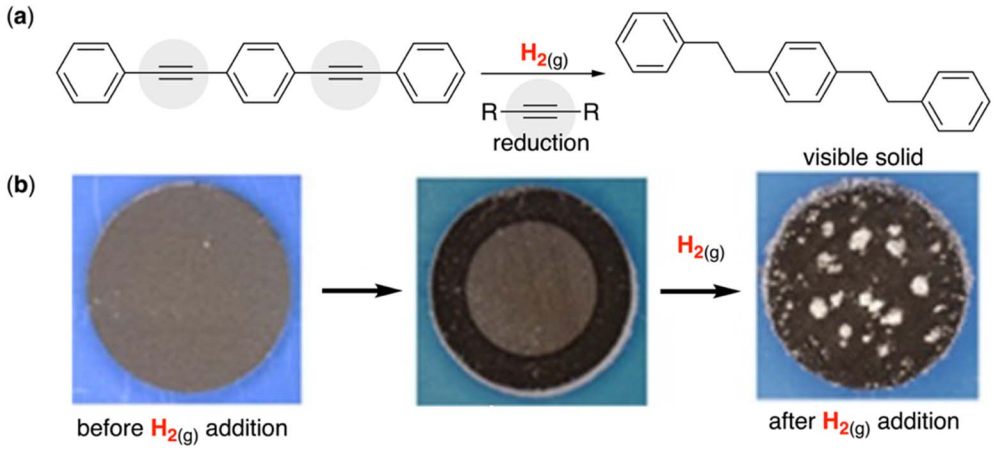

Fig. 2 (a) Structure of PEB before and after $H_{2(g)}$ exposure in the presence of Pd/C. (b) Cross section of PEB-Pd/C composite O-ring before (left), during (middle), and after (right) $H_{2(g)}$ exposure. Adapted with permission from ref. 68. Copyright © 2022 American Chemical Society.

platforms.[65] Of note, an $H_{2(g)}$ getter is a molecule capable of gettering $H_{2(g)}$, that is removing it from a closed system.[66] A recurring organic molecule used across Pd/C-based getter systems is 1,4-bis(phenylethynyl)benzene (PEB, also referred to as DEB). PEB contains multiple ethynyl functionalities that undergo irreversible hydrogenation in the presences of catalyst-activated $H_{2(g)}$, producing a saturated product with distinct physical and optical properties. This irreversible reactivity has been exploited in $H_{2(g)}$ scavenging applications to mitigate $H_{2(g)}$ accumulation. Notably, in several examples, visual changes arise even when the materials were not explicitly designed as optical $H_{2(g)}$ sensors. For example, Sangalang *et al.* reported rubberized PEB-Pd/C composite materials that function as an $H_{2(g)}$ getter, demonstrating effective and irreversible $H_{2(g)}$ uptake under mild conditions.[67] Upon $H_{2(g)}$ exposure, catalytic hydrogenation of PEB (Fig. 2a) led to the formation of white crystalline aggregates at the coating surface, providing a visual indication of $H_{2(g)}$ exposure. These optical changes originate from solubility differences between unreacted and hydrogenated PEB within the polymer matrix.[67] Similarly, Matt *et al.* incorporated PEB-Pd/C composite into O-ring seals, where $H_{2(g)}$ exposure again produced white crystalline precipitates due to hydrogenation of PEB (Fig. 2).[68]

Other work has intentionally leveraged PEB-Pd/C composite systems for optical detection of $H_{2(g)}$. Luzzatto *et al.* incorporated PEB and Pd/C into a polydimethylsiloxane (PDMS)-based polymer matrix for visual $H_{2(g)}$ detection.[69] Upon illumination with light (365 nm), the unreacted material appeared light blue in colour due to the presence of PEB. Once exposed to $H_{2(g)}$, the material displayed a purple colour localized at the surface due to $H_{2(g)}$ interaction. Spectroscopic analysis revealed a significant decrease in fluorescence intensity at 450 nm following 60 min of exposure to 500 mbar $H_{2(g)}$. A detection limit of 1000 ppm with a response time of >l min is reported. This system is proposed as a litmus-paper-like sensor, capable of recording $H_{2(g)}$ exposure history based on surface colour and penetration depth, functioning as an irreversible qualitative sensor.[69]

Despite their promise, Pd/C-based composite materials often provide qualitative data, limiting their utility in applications requiring precise $H_{2(g)}$ concentration measurements. A notable exception was reported by Zhou *et al.*, who showed quantitative fluorescence-based hydrogen detection using Pd/C in combination with the redox-active dye, resazurin (RZR).[70] In this system, the Pd–H produced from activation of $H_{2(g)}$, reduced weakly fluorescent RZR to strongly fluorescent resorufin (RSR). Solutions containing 10 μg of Pd/C and 25 μM RZR produced a fluorescence response at 580 nm over a wide $H_{2(g)}$ concentration range (0.2–80%), while remaining unresponsive to oxygen ($O_{2(g)}$), nitrogen ($N_{2(g)}$), argon ($Ar_{(g)}$), and $CO_{2(g)}$. The estimated detection limit was as low as 0.06% $H_{2(g)}$.[70] This system demonstrated low molar amounts of both activating agent and dye molecule required for effective fluorescence-based sensing. Mechanistic studies of these systems revealed that hydrogen spillover plays a dominating role. In this process, $H_{2(g)}$ undergoes dissociative adsorption on the Pd metal catalyst, followed by migration and diffusion of atomic hydrogen across the support, where it reacts with the organic molecule.[71] From this, it is evident that $H_{2(g)}$ solubility in the matrix and the diffusion of the reactants strongly influence the reaction rates, suggesting that special care must be taken in selecting both the matrix and the organic molecule to ensure the efficiency of these systems.

Together, these studies demonstrate the versatility of Pd/C nanocomposite materials for both solution-based and solid-state optical $H_{2(g)}$ detection. While the specific optical output, precipitation, colour change, or fluorescence change all depend on the choice of reporter molecule, the underlying mechanism is consistent across systems. In all cases, Pd activates $H_{2(g)}$ to generate surface bound hydrogen atoms, which are subsequently transferred to a reducible organic reported such as PEB or RZR, to produce an optical response. This highlights Pd/C as an effective and adaptable $H_{2(g)}$-activating platform that can be paired with a wide range of reducible dyes to tailor optical responses for specific $H_{2(g)}$ activation.

3.1.2. Nanoparticles. Noble-metal nanoparticles (NPs) provide a tuneable and versatile platform for surface-mediated $H_{2(g)}$ activation in dye-based optical sensing. In these systems, $H_{2(g)}$ is adsorbed at the NP surface to form reactive surface-bound metal-hydride species, which subsequently participate in redox reactions with organic dyes to generate an optical or fluorescence response, as described in this and previous sections. Among others, Smith *et al.* systematically investigated the use of bimetallic gold–palladium (Au–Pd) NPs combined with different indicator dyes to produce visually observable responses to $H_{2(g)}$.[72] In this study, Au–Pd NPs with diameters of ~18–25 nm were synthesized and employed as heterogeneous catalysts to dissociate $H_{2(g)}$ under ambient conditions, allowing for subsequent reduction of dissolved indicator dyes. Three indicator dyes were evaluated, including Bromothymol Blue, Methyl Red, and RZR. While both Bromothymol Blue and Methyl Red displayed visible colour and spectroscopic changes upon $H_{2(g)}$ exposure, these dyes were deemed unsuitable for the intended biomedical application due to slow response times and, in the case of Methyl Red, the formation of an acutely toxic biproduct. Nevertheless, these results demonstrate that Au–Pd NPs can be paired with a range of reducible dyes to elicit optical responses, highlighting the flexibility of this sensing strategy for different applications. The RZR/Au–Pd NP system displayed a rapid and pronounced optical response and was therefore further investigated. Weakly fluorescent RZR was reduced to highly fluorescent RSR, producing a distinct visible blue-to-pink colour change in solution with approximately 1 min of $H_{2(g)}$ exposure. After an additional 2 min of $H_{2(g)}$ exposure, RSR was further reduced to colourless dihydroresorufin (Fig. 3a).[72] The observation of this secondary reduction product, which was not reported with the Pd/C nanocomposite materials previously discussed, can be explained by enhanced absorption kinetics and solubility of Au–Pd NPs systems which may contribute to an increase in $H_{2(g)}$ activation.[60] Prolonged exposure of dihydroresorufin to air returned the pink colour, affording an "on–off"-type $H_{2(g)}$ sensor. A follow up study transitioned this NP-based sensor into a practical device format, developing thin, wearable, non-invasive optical sensors for monitoring $H_{2(g)}$ production from the degradation of Mg implants.[73] In this work, the Au–Pd NPs and RZR were embedded within a hydrogel matrix to create a flexible sensor capable of spatially resolved mapping of $H_{2(g)}$ released by observing a blue-to-pink colour change. An estimated limit of detection was determined to be between 8 and 6 μM, depending on the method used. The optical response was recorded using a smart phone camera, underscoring the practicality of NP-based dye sensors in real-world medical applications.[73]

Beyond Au–Pd NP systems, platinum (Pt) colloids have also been employed as effective $H_{2(g)}$ activating agents in dye-based optical detection. For example, McDonnell *et al.* reported a colorimetric $H_{2(g)}$ indicator film designed for detecting both gaseous and dissolved $H_{2(g)}$ under biologically relevant conditions, expanding dye-NP systems into practical encapsulated sensors.[74] This system utilizes the redox active dye MB in conjunction with Pt nanoparticles (~2.2 nm), immobilized within a hydroxyethyl cellulose matrix containing glycerol as a humectant and polysorbate as a surfactant. This mixture was dried onto a white Tyvek substrate and fully encapsulated between two 50 μm thick gas permeable low-density polyethylene (LDPE) sheets. $H_{2(g)}$ interacts with and is activated by Pt, reducing Methylene Blue to *Leuco*-Methylene Blue, producing a blue to colorless change in response to $H_{2(g)}$ and when the system was exposed to $O_{2(g)}$, the *Leuco*-Methylene Blue was oxidized back to Methylene Blue, giving on-off character to the sensor (Fig. 3b). Interestingly, the non-encapsulated film

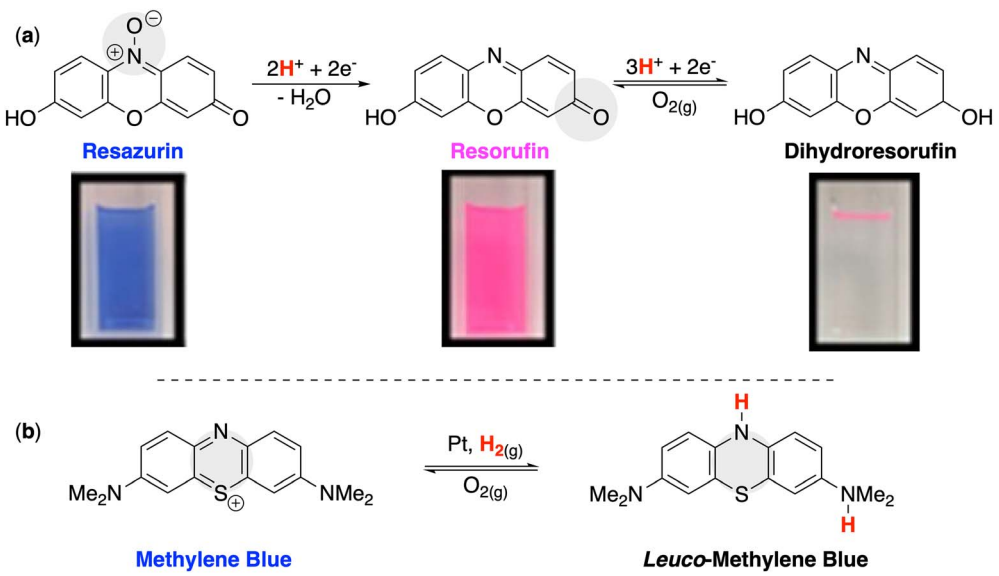

Fig. 3 (a) Redox reaction of resazurin upon reaction with $H_{2(g)}$ in the presence of a noble-metal catalyst with visual colours. Adapted with permission from ref. 72. Copyright © 2020 American Chemical Society. (b) Redox reaction of Methylene Blue upon reaction with $H_{2(g)}$ in the presence of a noble-metal catalyst. Adapted from ref. 74 with permission from the Royal Society of Chemistry.

showed a 50% response time to $H_{2(g)}$ of 0.3 min compared to 0.7 min for the encapsulated film with similar trends for $O_{2(g)}$ recovery. The indicator exhibits a response between 0.04 and 23.9% (v/v) $H_{2(g)}$ with a reported detection limit of 0.16% $H_{2(g)}$, while maintaining stability over 72 h in bacterial growth media. The laminated structure enables selective gas permeation while excluding biological and media contaminants, allowing direct immersion in microbial cultures. This platform was utilized to screen, by naked-eye or photographically, for $H_{2(g)}$ generating bacteria under anerobic conditions. High-throughput screening of $H_{2(g)}$ generating bacteria and quantitative determination of total viable cell count using micro-respirometry was also demonstrated.[74]

In an earlier study, Seo *et al.* demonstrated a simple method for determining dissolved $H_{2(g)}$ concentrations in water using Pt NPs in combination with Methylene Blue.[75] In this system, Pt NPs catalyze $H_{2(g)}$ dissociation in aqueous solution, enabling the reduction of blue MB, as described above. Although this approach was explored as an oxidimetric titration method, the visual colour loss in solution when exposed to $H_{2(g)}$ demonstrates the potential to use Pt NPs with an indicator dye for optical $H_{2(g)}$ detection.[75] Taken together, these studies demonstrate that noble-metal NPs, including Au–Pd and Pt-based systems, provide a platform for dye-based optical hydrogen detection. Across all implementations, the sensing mechanism remains consistent where $H_{2(g)}$ is activated at the NP surface and subsequently transferred to a redox-responsive dye, producing a measurable optical or fluorescence response. While NP-based dye sensors remain relatively underexplored, these examples highlight how observable colour change, response time, and application can be tuned through intentional selection of both NP catalyst and dye molecule. These findings establish noble-metal NPs as critical bridges between simple supported catalysts and SP architectures, as discussed in the following section.

3.1.3. Supraparticles. SPs are defined as particles composed of smaller building blocks held together through non-covalent interactions and capillary forces generated during fabrication.[59] In the context of $H_{2(g)}$ sensing, SPs represent a significant advancement over simple dye-NP dispersions, as they integrate all functional components into a single framework. This architecture enables precise control over $H_{2(g)}$ absorption and activation, as well as optical signal generation. Across all reported SPs systems for the optical detection of $H_{2(g)}$, a consistent design strategy is employed. Silica (SiO_2) NPs form a mechanically stable, mesoporous framework, whose structure defines its internal pore structure, gas permeability, and water retention.[76] Embedded within this framework are noble-metal NPs which serve as $H_{2(g)}$ activators *via* dissociative adsorption of $H_{2(g)}$, as discussed previously. Redox-responsive dyes are also retained within the framework in the presence of confined water. This architecture establishes an internal solid–liquid–gas interface, where $H_{2(g)}$ diffuses through the porous network, is activated at the noble-metal NP surface, and is subsequently reacted with the dye molecule to generate a visible optical response. Spray-drying is the universal fabrication method for the generation of SPs. In this process, colloidal dispersions are sprayed as aerosol particles and rapidly dried, forcing SiO_2 NPs, noble-metal NPs, and dye molecules into densely packed spheres.[59] This industrially-relevant technique allows for structural control on the SP size, porosity, and component distribution through variation of the individual components size, type, and concentration, as discussed below.

Reichstein *et al.* introduced the first fully integrated SP platform for dye-based optical detection of $H_{2(g)}$.[77] In their work, bimetallic Au–Pd catalytic NPs (~15–50 nm), SiO_2 NPs, and RZR were assembled into SPs *via* spray-drying. Upon exposure to a humid atmosphere, known as *ex situ* H_2O dosing, the SPs absorb water into their pore network, enabling dye mobility and facilitating hydrogen spillover from Au–Pd NP surfaces. Exposure to $H_{2(g)}$ induced the rapid, eye-readable purple-to-pink-to-colourless colour change associated with the RZR-to-RSR-to-hydroresorufin (hRF) reduction which occurs in a matter of seconds. Notably, this rapid visual response was achieved with low noble-metal NP loading (~0.04 wt%). A key mechanistic insight gained from this study was that confined water within the SP pores was essential for dye transport and sensor function; systems that were not H_2O-dosed did not respond to $H_{2(g)}$.[77]

Zhang *et al.* systematically evaluated the influence of noble-metal catalyst NP size and composition on SP performance, while maintaining SP architecture and dye loading.[78] The catalysts used included Pt, Pd, Au–Pd, and Au NPs, which were 2–5 nm, 10 nm, 20–40 nm, and 25 nm in diameter, respectively. Pt-based SPs exhibited the fastest response time, highest reaction capacity, and best reproducibility. Here, superior performance was attributed to small Pt NP size, minimal agglomeration, and high surface area accessible for dissociative $H_{2(g)}$ adsorption. In contrast, Pd-based SPs showed slower response time due to $H_{2(g)}$ absorption and formation of Pd hydride (PdH_x), reducing available activated hydrogen on the NP surface. Au NPs were incapable of activating $H_{2(g)}$. These results established that catalytic surface availability, rather than total $H_{2(g)}$ uptake capacity, is the dominant parameter governing SP-based optical $H_{2(g)}$ detection efficiency.[78] A related study further emphasized the importance of pore hydrogenation and NP dispersion, demonstrating that well-dispersed Pt NPs within hydrated SPs enable $H_{2(g)}$ detection at concentrations an order of magnitude below its lower flammability limit (4 vol%).[79] Together, these studies define catalyst identity, NP size, and water content as primary design variables for SP-based $H_{2(g)}$ sensors.

Reichstein *et al.* further advanced the SP platform through a systematic multivariable optimization of SiO_2 NP size, catalyst loading, and dye identity/concentration (Fig. 4).[80] By reducing the SiO_2 NP size from bimodal 20–90 nm NP systems down to 8 nm, SPs exhibited an 87% decrease in response time and ~3-fold faster recovery. The improvement was attributed to increased surface area, smaller pores, and enhanced water uptake, which collectively improved dye mobility and $H_{2(g)}$ transport. Increasing Pt NP concentration from 0.009 wt% to 0.0442 wt% reduced response time by 97% due to increased availability of $H_{2(g)}$ activation sites. However, excess Pt NP loading reduced optical response due to light absorbance and scattering, identifying an optimal loading window between

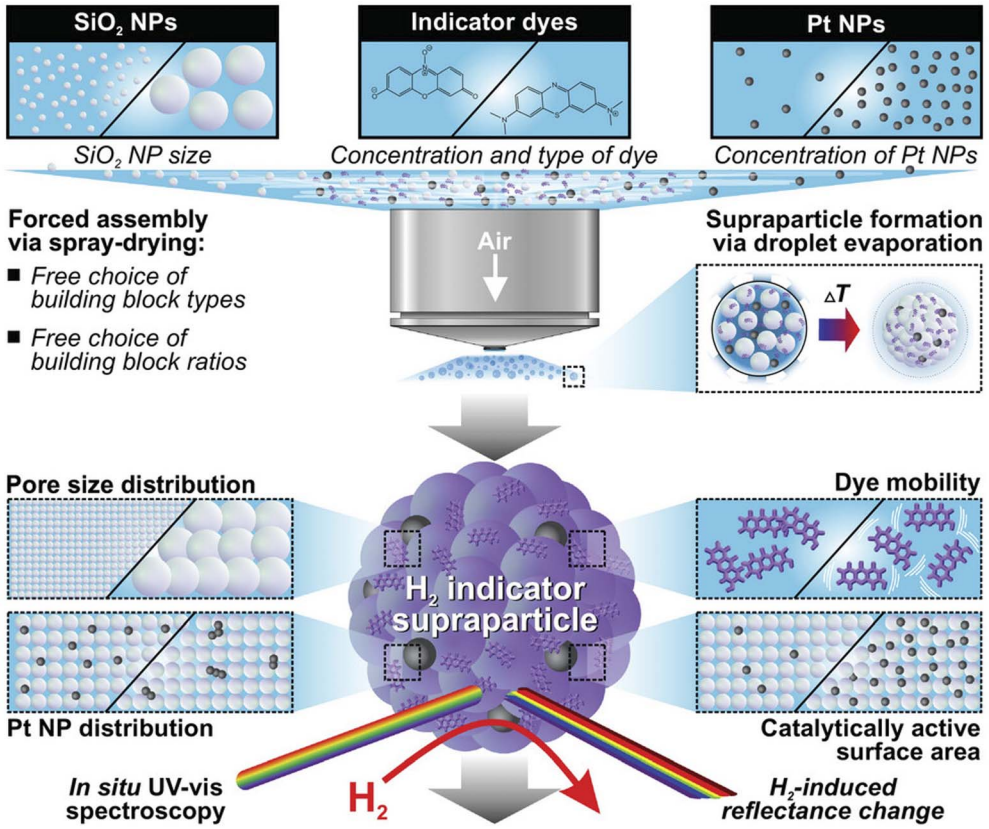

Fig. 4 Customizable components of $H_{2(g)}$ indicator supraparticles and key characteristics that dictate their performance. Adapted from ref. 80, copyright © 2024 Wiley-VCH GmbH.

0.04–0.08 wt%, demonstrating that careful optimization of loading concentration is required for optimal response. Variation of dye concentration revealed similar trade-offs, increasing RZR concentration to 0.05 wt% maximized optical contrast, while maintaining rapid kinetics; excessive dye loading reduced transport efficiency and slowed response. Importantly, the SP platform provides an opportunity to vary the reporter dye molecule such as RZR, Methylene Blue, dichloroindophenol, Methyl Red, and tetrazolium red, enabling customizable optical outputs. These findings establish SPs as a tunable sensing platform in which pore structure, catalyst identity/loading, and dye concentration/identity can be independently optimized. This study also provides insight into the number of optimization factors that can be altered to achieve optimal $H_{2(g)}$ response.

Zink *et al.* extended the SP platform beyond single gas detection by incorporating H_2SO_4 into Pt-based (5–10 nm) SPs to enable dual gasochromic detection of $H_{2(g)}$ and ammonia (NH_3).[81] Sulfuric acid (H_2SO_4) incorporation resulted in the protonation of purple RZR to orange RZR-H^+, enabling $H_{2(g)}$ and pH-dependent colour transitions. Upon $H_{2(g)}$ exposure, Pt-mediated $H_{2(g)}$ activation reduced orange RZR-H^+ to the brighter protonated resorufin (RSR-H^+) and subsequently to blue hRF$^\bullet$, a radical intermediate en-route to colourless hRF (Fig. 5a). This full conversion from RZR-H^+ to hRF takes about 5–10 s. In contrast, NH_3 exposure induced rapid (~3 s) deprotonation induced colour change from orange RZR-H^+ to purple RZR (Fig. 5b). However, NH_3 was shown to poison Pt catalytic activity, preventing $H_{2(g)}$ detection under simultaneous or successive exposure. This study demonstrates that the composition of the liquid confined within SP pores can be engineered to introduce parallel sensing pathways. Additionally, the choice of dye is an important consideration as pH sensitive dyes, depending on environment, can elicit non-specific detection and change of signal.[81]

Until now, all SP systems discussed have used powders produced by spray drying. Wenderoth *et al.* advanced the SP-based $H_{2(g)}$ sensing platform from these powders to mechanically robust composites.[82] SiO_2-Pt-RZR SPs, in the form of powder, were embedded into a poly(methyl methacrylate) (PMMA) matrix to produce millimeter-scale suprabeads and self-supporting films (Fig. 6). An optimized composition containing 99.9 wt% SiO_2, 0.05 wt% Pt NPs, and 0.05 wt% RZR preserved the characteristic purple-to-pink-to-colourless transition across all formats. Suprabeads retained gas accessibility and detected $H_{2(g)}$ down to 0.1 vol% within minutes, well below its lower flammability limit. Thin films (~131 nm thickness) exhibited a slower response limited by $H_{2(g)}$ diffusion, requiring higher concentrations or longer exposure times. This study demonstrates that SP architecture can be engineered into durable formats suitable for capillary flow systems and direct pipeline leak detection, both relevant to real-world

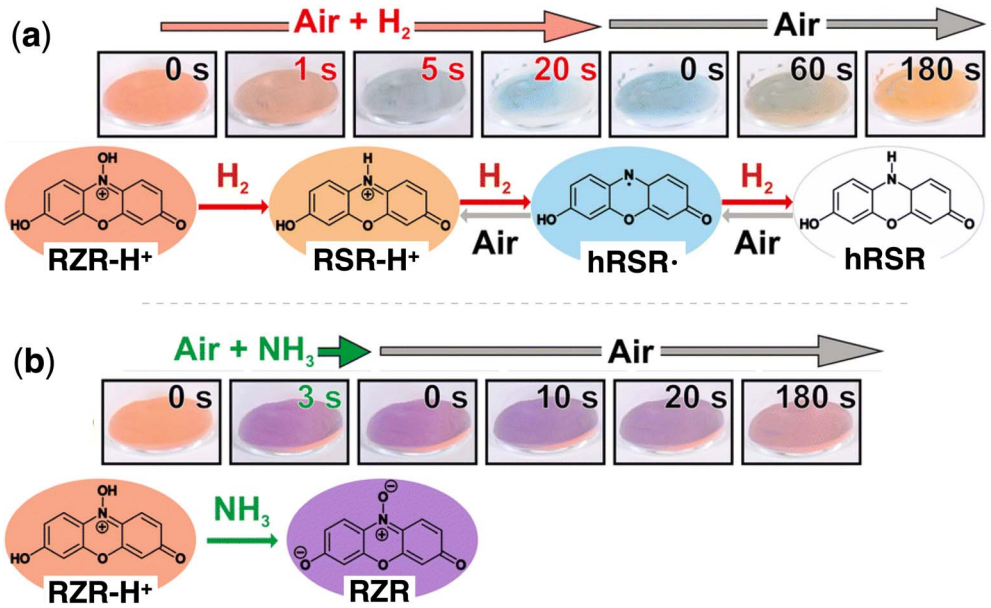

Fig. 5 (a) Redox reactions of protonated RZR-H^+ when exposed to $H_{2(g)}$ or air within supraparticle powders containing Pt nanoparticles with H_2SO_4 added. (b) Deprotonation of RZR-H^+ to RZR upon exposure to NH_3 within supraparticle powders containing Pt nanoparticles with H_2SO_4 added. Adapted from ref. 81 with permission from the Royal Society of Chemistry.

applications.[82] Future work could explore alternative matrices and formats to improve reaction time. These SP studies establish several clear design principles for optical $H_{2(g)}$ sensing. First, efficient performance depends on maximizing the availability of surface-active $H_{2(g)}$ at noble-metal NPs, with small, well-defined Pt NPs providing fast and reproducible responses. Second, pore structure and water retention within SiO_2 framework are crucial, as confined water enables dye mobility. Finally, catalyst and dye concentration must be balanced to optimize response time and optical signal. From these studies, it has been demonstrated that SP optical $H_{2(g)}$ sensing is governed by an intricate interplay of multiple components within a single structure.

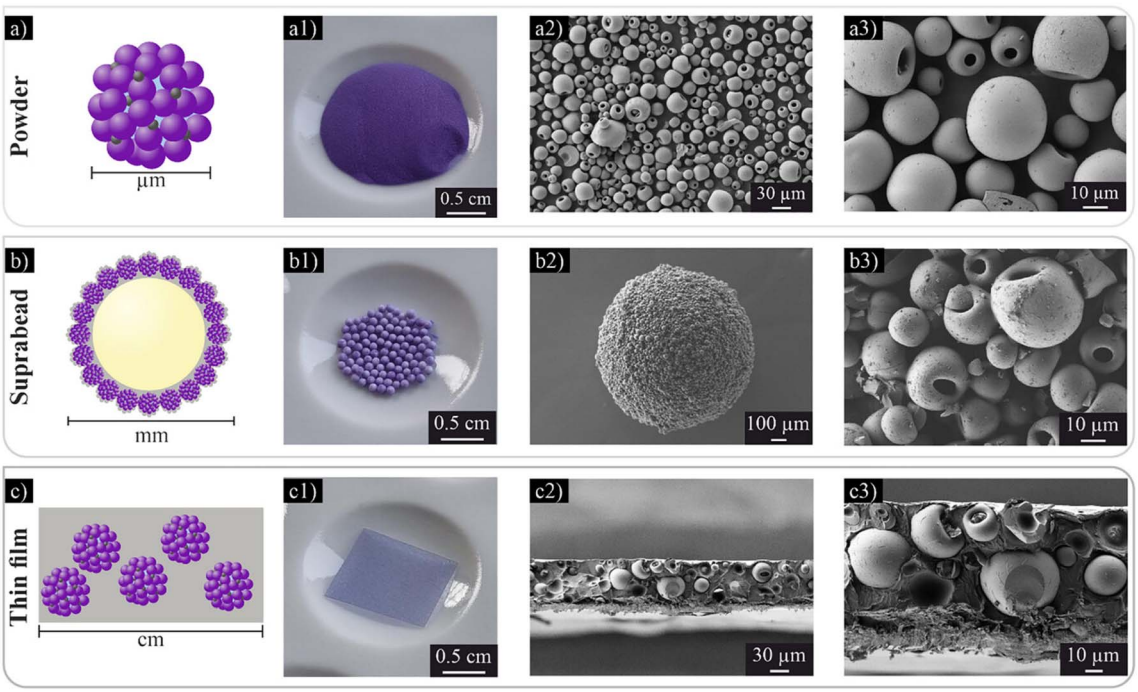

Fig. 6 Illustration of three different fabrications: (a) powder, (b) suprabeads, (c) self-supporting thin films. (1) Photographs of the assemblies and (2 & 3) SEM images. Reproduced from ref. 82, copyright © 2026 Wiley-VCH GmbH.

3.2. Organometallic complex activation of hydrogen gas for dye-based optical sensing

Organometallic complexes have been employed as $H_{2(g)}$ activation partners in dye-based optical sensors. In these systems, $H_{2(g)}$ directly reacts with the organometallic complex, most often a rhodium (Rh) or iridium (Ir)-based complex, giving a M–H unit that can be used for dye reduction.[35–37] Although the activation mechanism differs slightly from surface mediated noble-metal NP systems, the fundamental process remains the same: activation of $H_{2(g)}$ followed by transfer of the reactive hydrogen species to a dye molecule, resulting in a detectable optical response. While having less precedent than NP-based systems, these sensors provide structural tunability as well as valuable insight into fundamental $H_{2(g)}$ activation, offering a complimentary sensing strategy for optical $H_{2(g)}$ detection.

3.2.1. Rhodium-based catalysts. Wilkinson's catalyst, chemically known as tris(triphenylphosphine)chlororhodium(I), was first reported in 1964 as an efficient catalyst capable of activating $H_{2(g)}$ for hydrogenation reactions.[83] This compound readily undergoes reversible interactions with $H_{2(g)}$, forming reactive Rh-hydride species capable of transferring hydrogen to unsaturated organic substrates. Subsequent work led to the development of sulfonated, water-soluble derivatives of Wilkinson's catalyst that retained hydrogenation activity, expanding potential applications.[84] Katsuda *et al.* reported one of the earliest examples of optical $H_{2(g)}$ detection based on an organometallic molecule coupled with an organic indicator dye.[85] In this study, the authors explored the hydrogenation ability of a water-soluble sulfonated Wilkinson's catalyst derivative to develop a screening method for $H_{2(g)}$-producing microorganisms. The rationale was that hydrogenation (saturation) of a conjugated dye would result in a visible colour change. In this system, $H_{2(g)}$ generated by $H_{2(g)}$-producing microorganisms in sealed culture vessels dissolved in water were amenable to activation by the catalyst. The generated Rh–H then hydrogenated the indicator dye, producing a visible colour change that was correlated to $H_{2(g)}$ production. A variety of indicator dyes were evaluated including Methylene Red, Nile Blue, Neutral Red, Methyl Orange, Methyl Red, Crystal Violet, Victoria Blue, Evans Blue, Coomassie Brilliant Blue, Bromophenol Blue, Eriochrome Black T, Thymol Blue, Orange II, Phloxine B, and Rhodamine B. Nearly all dyes produced a noticeable colour change upon $H_{2(g)}$ exposure in the presence of the Rh complex at room temperature, demonstrating breadth

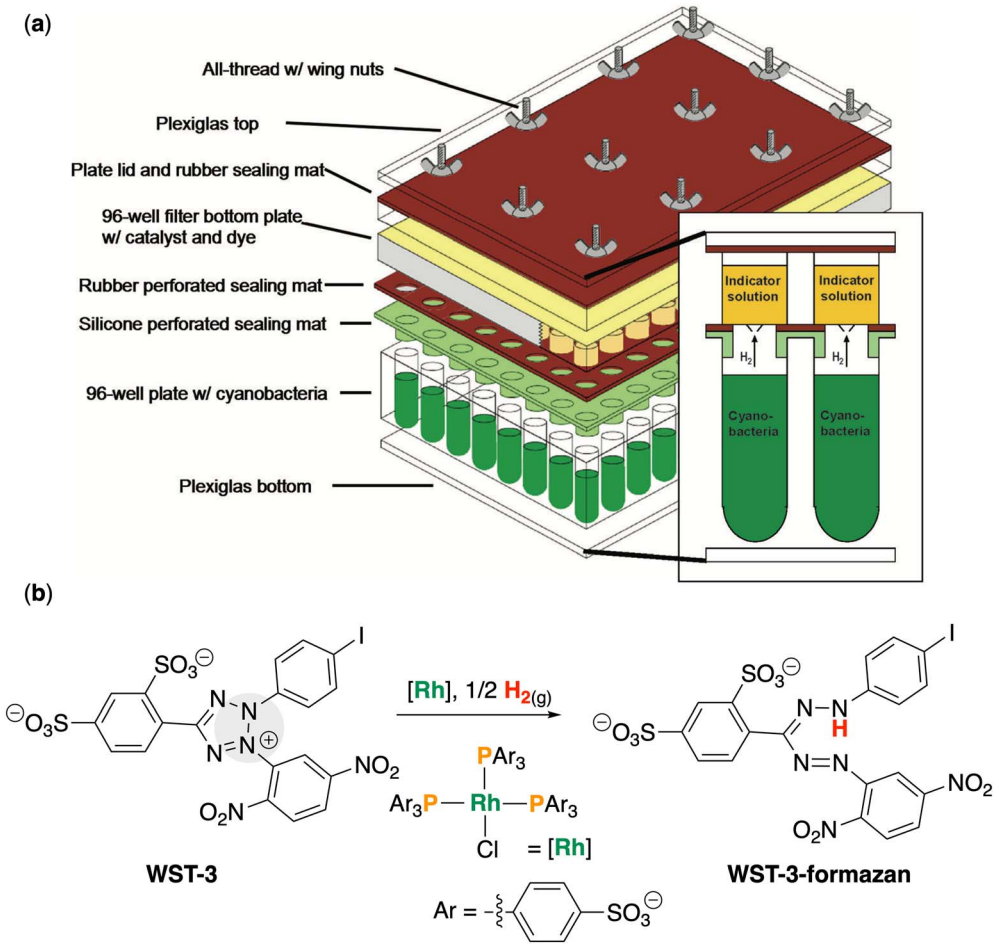

Fig. 7 (a) A diagram of the high-throughput screening assay and (b) the reaction of WST-3 with $H_{2(g)}$ catalyzed by sulfonated Wilkinson's catalyst to form WST-3 formazan. Adapted with permission from ref. 86. Copyright © 2008 American Chemical Society.

of approach. The authors chose the Methyl Orange system for this assay as it demonstrated good reaction time, colour change, and low inhibitory effects on the cells. Importantly, the catalyst functioned as an efficient $H_{2(g)}$ activator, leading to an optical signal generation without NPs or elevated temperature. However, in this assay, cumulative $H_{2(g)}$ was detected over a 3–5-day period which may be due to the slow production of $H_{2(g)}$ by the microorganisms. This study was not framed as a general $H_{2(g)}$ sensor, but it established a foundational method showing that $H_{2(g)}$ can be activated by a homogeneous metal-catalyst to produce an optical response from an indicator dye.[85]

Building on this work, Schrader *et al.* developed a high-throughput (Fig. 7a) optical assay for detecting biologically produced $H_{2(g)}$ utilizing a similar catalyst-dye system.[86] In this work, $H_{2(g)}$ generated by microorganisms was transferred into the aqueous phase, where it was activated, allowing for subsequent hydrogenation of an indicator dye, producing a measurable optical response (Fig. 7b). A variety of indicator dyes were evaluated including water-soluble tetrazolium (WST-1, WST-3, WST-5, WST-9, and WST-11), Methyl Orange, Methylene Blue, and Methyl Purple. In parallel, multiple catalysts were investigated including sulfonated Wilkinson's catalyst as well as a series of Ir, Rh, and ruthenium complexes having sulfonated triphenylphosphine ligands. Among the combinations tested, WST-3 with the sulfonated Wilkinson's catalyst provided the most reliable and sensitive response for biological screening. Importantly, this systemic evaluation demonstrated that both dye and organometallic complex structure can be varied to tune optical $H_{2(g)}$ sensor performance. Of note, the reaction time varied between 1.5–185 h, which is non-ideal for application as an industry-applicable sensor. However, the authors note that the reaction of the dye with the catalyst is much faster than $H_{2(g)}$ evolution from the solution. Nonetheless, this study advances our understanding of the intricate roles of organometallic complexes and dyes by emphasizing practical, quantitative, and high-throughput methods that leverage catalyst-dye combinations.

3.2.2. Iridium-based catalysts. Recent Ir catalyst-based fluorescence $H_{2(g)}$ sensors represent a modern re-emergence of the organometallic catalyst strategy, revisiting the principles of the earlier Rh-based systems while transitioning them to more conventional analytical sensing formats. Unlike the Rh-based assay platforms developed for biological screening, Ir-based systems have been explicitly designed for optical $H_{2(g)}$ sensing, typically employing fluorescent dyes that offer improved sensitivity and compatibility with practical sensing formats. Kos and Plenio introduced a fundamentally new approach to $H_{2(g)}$ detection by attaching a fluorophore directly onto a $H_{2(g)}$-activating Ir complex, thereby creating a single-component fluorescent molecular probe for $H_{2(g)}$.[87] This work exploits changes in metal-center electron density induced by $H_{2(g)}$ activation to modulate the fluorescence intensity of the appended dye molecule. This work stemmed from the authors previous study in which a series of transition-metal complexes based on Ru, Rh, Ir, Pd, or Au were functionalized with fluorescent tags, revealing that variation in metal electron density strongly influenced fluorescence emission of the appended fluorophore.[88] In their most recent work, a Crabtree-type Ir(I) hydrogenation catalyst was linked to a BODIPY (4,4-difluoro-4-bora-3*a*,4*a*-diaza-*s*-indacene) fluorophore *via* an N-heterocycle carbene linker to give the three weakly fluorescent Ir-containing compounds **1**, **2a**, and **2b** (Fig. 8). BODIPY dyes are strongly UV-absorbing fluorescent molecules with high quantum yields that are stable and relatively unaffected by their environments.[89] In the absence of $H_{2(g)}$, these complexes were weakly fluorescent and upon exposure to $H_{2(g)}$, oxidative addition at the Ir(I) center generated their respective Ir(III) dihydride containing compounds, producing a pronounced fluorogenic "turn-on" response (Fig. 8). This oxidative addition reaction occurred under ambient conditions in solution, reaching saturation within minutes. The probe enabled both visual and spectroscopic detection of $H_{2(g)}$, with a concentration dependent fluorogenic response between 1–4 vol% $H_{2(g)}$ when impregnated with propylene carbonate on filter paper. Beyond sensing, this study showed that fluorescence can serve as a direct reporter of early catalytic hydrogenation steps. Collectively, this work represents the first true molecular fluorogenic $H_{2(g)}$ sensor and established Ir-based organometallic complexes as a platform for dye-based optical $H_{2(g)}$ detection. Importantly, it was demonstrated that single molecule systems containing

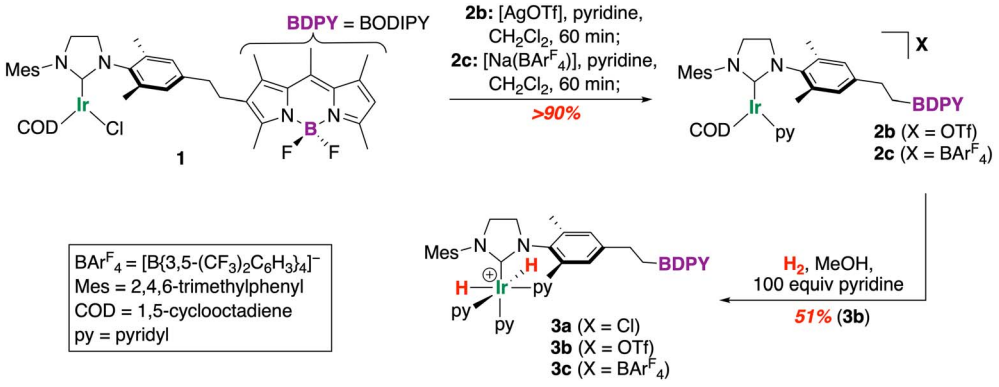

Fig. 8 Weakly fluorescent BODIPY-Ir complexes (compound **1**, **2a**, and **2b**) and their respective fluorescent Ir(III) derivatives (compound **3a**, **3b**, and **3c**). Adapted with permission form ref. 87. Copyright © 2015 WILEY-VCH Verlag GmbH & Co. KGaA, Weinheim.

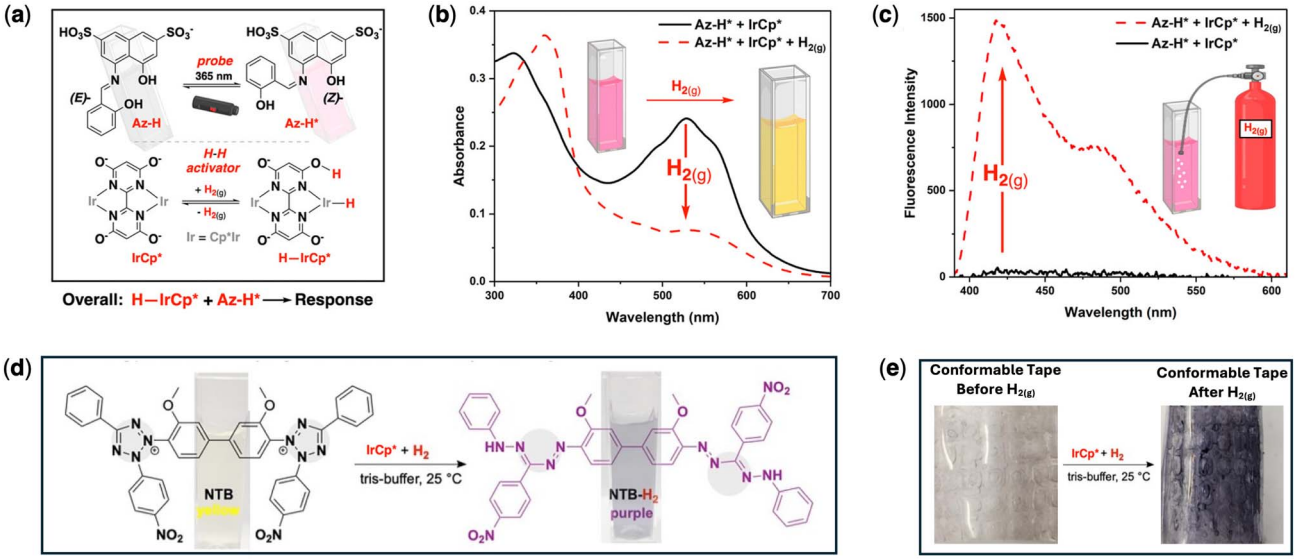

Fig. 9 (a) Structures of *trans*-azomethine-H (Az-H) and *cis*-Az-H*, top left to right, respectively, and structure of IrCp* before and after hydride complex (H–IrCp*) formation (bottom). (b) Change in the absorbance spectrum of the Az-H* + IrCp* solution ± $H_{2(g)}$. (c) Change in the fluorescence spectrum of the Az-H* + IrCp* solution ± $H_{2(g)}$. Adapted with permission from ref. 90. Copyright © 2025 American Chemical Society. (d) Chemical reaction of Nitrotetrazolium Blue with IrCp* to form the purple formazan product when exposed to $H_{2(g)}$, with structures. (e) Photos of the reaction mixture encapsulated in PDMS before and after $H_{2(g)}$. Adapted with permission from ref. 93. Copyright © 2025 American Chemical Society.

organometallic catalysts appended with fluorophores can provide significant responses to $H_{2(g)}$.[87]

Building from this report, a recent study by Potter *et al.* introduced an analogous intermolecular fluorogenic $H_{2(g)}$ sensor having a dye and Ir-based $H_{2(g)}$ activator.[90] In this system, the readily available naphthalene-based dye, azomethine-H (Az-H, 4-hydroxy-5-(2-hydroxy-benzylideneamino)-naphthalene-2,7-disulfonic acid) was combined with a water soluble Ir catalyst to create a hybrid molecular sensing platform capable of operating under ambient conditions (Fig. 9a). The Ir catalyst used, $[\{Ir(Cp^*)(Cl)\}_2(thbpym)]Cl_2$ (IrCp*, ($Cp^* = C_5Me_5^-$, thbpym = 4,4′,6,6′-tetrahydroxy-2,2′-bipyrimidine)) known here as "IrCp*" was originally synthesized by Hull *et al.* for the reduction of CO_2 into formic acid (FA) using $H_{2(g)}$ as a reductant in aqueous solution.[91] In an earlier study by Potter *et al.*, the indirect detection of $H_{2(g)}$ was proposed by coupling their novel FA sensors based on Az-H with a catalyst capable of producing FA from $H_{2(g)}$, such as IrCp*.[92] This work demonstrated the ability to detect $H_{2(g)}$ by first converting it to a more reactive species, opening avenues for future work related to detecting $H_{2(g)}$ through indirect methods. In their more recent study, the authors combined the oxidative addition and hydride-transfer steps of the FA-forming catalytic cycle to induce a fluorogenic response in Az-H. This work established a mechanistically defined, multistep sensing pathway in which photoquenching of Az-H to its non-fluorescent photoisomer Az-H* is followed by Ir-mediated $H_{2(g)}$ activation and subsequent hydride transfer to the dye, yielding a fluorogenic response. This work confirms that catalysts capable of CO_2 reduction can be integrated into dye-based systems for $H_{2(g)}$ detection applications. Due to the nature of the reaction, this sensor was not reversible and required the presence of some amount of water as a solvent to proceed. Either way, the sensor exhibited a ~47-fold fluorescence enhancement in solution accompanied by a colour change (Fig. 9b and c). This sensor can detect $H_{2(g)}$ concentrations as low as 0.5% with no cross-reactivity towards $N_{2(g)}$ or air. A readable signal was generated within ~5 s of $H_{2(g)}$ exposure, with saturation occurring within minutes. The sensing chemistry was successfully translated into a solid-state format by incorporation into a carboxymethylcellulose (CMC) hydrogel, which retained reactivity towards $H_{2(g)}$ and demonstrated potential for practical sensing applications. The authors further demonstrated the generality of this strategy by applying the same IrCp* catalyst to a functionally related naphthalene dye, H-acid (4-hydroxy-5-aminonaphthalene-2,7-disulfonic acid), confirming that this platform is compatible with multiple dyes. This work established a new subclass of dye-based optical $H_{2(g)}$ sensors in which the organometallic catalyst and dye remain separate, highlighting the potential to pair a variety of $H_{2(g)}$ activating catalysts with suitable dyes to create modular and tunable optical $H_{2(g)}$ sensors.[90]

Fisher *et al.* subsequently expanded the IrCp*-mediated $H_{2(g)}$ sensing strategy by pairing the same water-soluble catalyst, IrCp* with Nitrotetrazolium Blue (NTB), a redox-active dye, to develop a rapid and visually readable colorimetric $H_{2(g)}$ sensor.[93] In this sensor, IrCp* activated $H_{2(g)}$ under ambient conditions to generate reactive hydride species, which then reduced NTB to a blue-coloured formazan product, readily observable by the naked eye (Fig. 9d). This reaction mixture was encapsulated into a PDMS membrane allowing for generation of a tape-like system (Fig. 9e), making it particularly suitable for leak detection applications especially due to the irreversible nature of the

reaction. The PDMS encapsulation prevents water evaporation, elongating the sensors lifetime while maintaining $H_{2(g)}$ permeability. The encapsulated senor demonstrated rapid colour change under ambient conditions and could detect as low as 100 ppm $H_{2(g)}$ selectively with the use of a simple camera. Optical response occurred only in the presence of both IrCp* and NTB, confirming that $H_{2(g)}$ activation at the metal center is required for signal generation. By translating $H_{2(g)}$ activation chemistry into a deployable colorimetric format with strong visual contrast, this study further validates Ir organometallic complexes as efficient $H_{2(g)}$ activating agents and again highlights the versatility of catalyst-dye hybrid strategies for tailoring sensor applications and optical outputs.[93]

Organometallic-based $H_{2(g)}$ sensors demonstrate how $H_{2(g)}$ activation can be coupled to optical and fluorescence signal generation and are complimentary to surface-mediated platforms. Across all discussed Ir-based platforms, $H_{2(g)}$ activation occurs through oxidative addition at the metal center to form metal hydride species. These hydrides either directly influence the optical properties of an appended dye fluorophore or are transferred to a dye molecule to provide an optical response. At the same time, these systems highlight potential limitations of metal complex-based $H_{2(g)}$ sensors such as moisture sensitivity that can influence catalyst performance and long-term stability. In addition, catalyst poisoning has not been systematically investigated. The studies available on this topic are mostly conducted in solution or hydrogel matrices, and translation into deployable sensing devices remain at a proof-of-principle stage, requiring further development for industrial use. Additionally, the use of organometallic complexes that do not utilize noble metals (such as cobalt,[94] nickel,[95] and iron[96] complexes) would be highly desirable to further lower the overall cost of the sensor. Despite these challenges, organometallic complexes offer mechanistic clarity and chemical tunability, enabling signal generation to be modified through choice of catalyst and dye selection easily. These systems bridge fundamental hydrogenation catalyst chemistry and optical detection, providing valuable design insights for future hybrid $H_{2(g)}$ sensing techniques.

Table 1 compiles key performance parameters of representative optical dye-based $H_{2(g)}$ sensors discussed throughout this review, including reported limits of detection, concentration ranges, and response times. When examined collectively, the data reveals significant variability not only in sensor performance but also in how these parameters are defined and reported. In several studies, detection limits are implied rather than calculated, response times are present without clear definitions (*i.e.*, onset *vs.* t_{90}) or parameters under which response times were gathered, and experimental parameters such as $H_{2(g)}$ concentration are reported in various ways (*i.e.*,

Table 1 Overview of sensing parameters for dye-based optical hydrogen gas sensors

$H_{2(g)}$ activator	Dye molecule	Concentration range	Limit of detection	Response time	Detection method	Reversible	Ref.
Pd/C	1,4-Bis(phenylethynyl) benzene	1–500 mbar	1000 ppm (after 1 h)	<1 min (at 500 mbar)	Fluorescence	No	69
Pd/C	Resazurin	0.2–80% (v/v)	0.06% (v/v)	~15 min	Fluorescence	No	70
Au–Pd in solution	Resazurin	19.5–800 μM (dissolved)	6–8 μM (dissolved)	2 min (onset, >37.4 μM) 25 min (end point)	Colorimetric	Yes	73
Pt NPs in solution	Methylene blue	0.04–23.9% (v/v)	0.16% (v/v)	t_{50} = 0.3 min (naked) or 0.7 min (laminated) at 23.9% (v/v)	Colorimetric	Yes	74
Pt NPs (within SPs)	Resazurin	0.2–3.5% (v/v)	0.2% (v/v)	23 s (2% v/v) 296 s (0.2% v/v)	Colorimetric	Yes	80
Pt NPs (within SPs)	Resazurin	Not provided	2% (v/v)	5–10 s	Colorimetric	Yes	81
Pt NPs (within SPs)	Resazurin	0.2–66% (v/v)	0.2% (v/v)	t_{90} = 145 min (0.2% (v/v)) 8.5 min (1% (v/v)) 0.1 min (66% (v/v))	Colorimetric	Yes	78
Pt NPs (within SP powder, suprabeads, and thin films)	Resazurin	0.1–95% (v/v)	0.1% (powder and suprabeads) 1% (thin films)	Endpoint = <5 min (powder) and 8 min (suprabeads) for 0.1% (v/v); 10 min (thin film) for 1% (v/v)	Colorimetric	Yes	82
Sulfonated Wilkinson's catalyst	Methyl orange	760–7.6 μM (dissolved)	7.6 μM (dissolved)	50 h (endpoint)	Colorimetric	No	85
Sulfonated Wilkinson's catalyst	Water soluble tetrazolium-3	0–0.82 μmol (dissolved)	20 nmol (dissolved)	>12 h	Colorimetric	No	86
Crabtree-type Ir complex	BODIPY	1–4% (v/v)	1% (v/v)	4 min (endpoint)	Fluorescence	Yes	87
$[\{Ir(Cp^*)(Cl)\}_2(thbpym)]Cl_2$	Azomethine-H	0.5–10% (v/v), pure $H_{2(g)}$	0.5% (v/v)	5 s (onset) 5 min (endpoint)	Fluorescence	No	90
$[\{Ir(Cp^*)(Cl)\}_2(thbpym)]Cl_2$	Nitrotetrazolium blue	0.01–1% (v/v), pure $H_{2(g)}$	0.01% (v/v)	10 s (pure $H_{2(g)}$) 5 min (1% (v/v)) >10 min (0.1% (v/v))	Colorimetric	No	93

concentration, ppm, or dissolved). This complicates direct comparison across platforms and acts as a bottleneck for the determination of optimal sensor design and sensing parameters for future sensors generations. Accordingly, future studies should clearly define limit of detection and working concentration range ideally in terms of ppm and $H_{2(g)}$% (v/v), response times (onset for observable change and t_{90} for reaction completion), recovery times (if reversible), operating conditions (temperature, humidity, gas composition, and flow rate). By standardizing the format in which these parameters are reported, the rational development of next generation optical dye-based $H_{2(g)}$ sensors can be accelerated.

4 Conclusion and future perspectives

Fluorescent and optical dye-based $H_{2(g)}$ sensors have evolved through several distinct, yet connected strategies, all of which rely on indirect chemical activation of $H_{2(g)}$ by a metal to generate an optical response. Early systems based on Pd/C composites and noble-metal NPs established the use of surface-mediated $H_{2(g)}$ activation. Later advancements incorporated NPs into SP architectures allowing careful control over catalyst dispersion, pore size, and dye loading which drastically altered sensitivity, response time, and optical read out. More modern $H_{2(g)}$ sensors utilized organometallic complexes for $H_{2(g)}$ activation and sensing.

Pd/C composites are most often used in $H_{2(g)}$ getter technology to mitigate leakages. These systems can generate precipitates giving a qualitative indication of $H_{2(g)}$ presences. In addition, Pd/C composites have been paired with dyes to quantitatively detect $H_{2(g)}$. NPs based on Au–Pd and Pt have both been used as $H_{2(g)}$ activators paired with a variety of dyes to produce colorimetric and fluorescence responses to $H_{2(g)}$. These systems provide evidence that parameters such as dye identity can be changed, altering sensing performance, but maintaining $H_{2(g)}$ detection, providing a tailorable system. SP assemblies provide a large data set on how architecture, noble metal catalyst composition, size, and concentration, dye identity, and concentration all have drastic effects on the optical response generated and efficiency of $H_{2(g)}$ detection, providing meaningful data to enhance future designs. For example, small Pt-based catalysts are most efficient at $H_{2(g)}$ activation and RZR is the most widely use dye for $H_{2(g)}$ sensing. However, other parameters such as NP and dye concentrations must be optimized as too much or too little leads to reduced response, and pour size plays a significant role in $H_{2(g)}$ uptake. Across all surface-mediated systems, $H_{2(g)}$ is activated at the surface of the metal catalyst before reducing the dye molecule to generate an optical response.

In contrast, organometallic complex-based sensors represent a fundamentally different approach, in which $H_{2(g)}$ activation occurs at a coordinated metal center. Rh and Ir are the most popular types of catalysts employed in literature due to their near-ideal $H_{2(g)}$ adsorption energy, tunable electronic structure, and stability across pH ranges, with other catalysts showing potential.[97] These systems can be directly coupled to dye hydrogenation or direct signal changes, providing highly tunable optical responses. Ir-based platforms demonstrate how oxidative addition and hydride transfer chemistry can be repurposed from traditional hydrogenation catalysis into optical signal transduction. This provides potential evidence that a large range of organometallic catalysts that operate under relevant conditions can be repurposed for $H_{2(g)}$ sensing strategies. Of particular interest are complexes that are based on more abundant metals such as cobalt,[94] nickel,[95] and iron[96] which have been reported but not yet employed in the context of $H_{2(g)}$ sensing.[34,98] However, the use of these metals are still challenging due to their low efficiency in terms of their turn over frequency, reaction rate under mild conditions, reactivity, and reaction procedures when compared to noble metal catalysts.[98] In addition, noble metals are air and moisture stable, and have predictable two-electron chemistry which is absent for 1st row d-block metals.[99,100] Moreover, there is sufficient evidence that most redox active dyes can be utilized to provide a readable signal and the signal generated and usability depends largely on the optical properties of the dye before and after reduction. Compared to surface mediated systems, organometallic complex-based systems require lower metal loading and allow signal generation to be rational engineered though catalyst and dye selection with less influence from material architecture.

Looking forward, both surface mediated and organometallic hybrid sensing strategies should be further developed as complimentary approaches to optical $H_{2(g)}$ sensing. While current solid-state sensors predominantly rely on Pd/C composites and noble metal-based NP, future research should explore immobilizing organometallic complexes within polymers or SP platforms to retain molecular control while improving stability, scalability, and processability. This would further simply these systems by removing the current need for solvent for sensing. In parallel, expanding the library of $H_{2(g)}$ responsive dyes, especially fluorescent dyes, and exploring how to make their interaction with these catalysts reversible will be critical for advancing dye-based detection. The use of RZR or Methylene Blue with $H_{2(g)}$ activators to achieve on-off dye-based sensing, is particularly promising. In addition, alternative catalysts for the conversion of $H_{2(g)}$ into chemically reactive species for its indirect detection may open avenues for $H_{2(g)}$ sensing not yet considered. Dyes that combine fluorescence and visible absorbance changes should be given special attention, as they enable both quantitative and qualitative signal generation within a single sensor.

All new sensors should be benchmarked against established performance parameters for effective $H_{2(g)}$ detection, including sensitivity below the lower flammability limit (4% v/v), work over relevant temperatures ranges (−30 to 80 °C) with rapid response time (~1 s) and a long-term stability. Sensors should also be evaluated for cross-reactivity to common contaminants and interferents (hydrocarbons, carbon monoxide (CO), CO_2, O_2, hydrogen sulfide (H_2S), NH_3, *etc.*), shelf life, and when applicable, reversibility, cycling, and hysteresis. For quantitative systems, standard calibration curves and limit of detection must be reported, along with protocols use to generate them.

To enable direct comparison across optical dye-based $H_{2(g)}$ sensor studies, the field would benefit from standardized

reporting of key parameters. At minimum authors should report (i) the detection limit (with defined and calculated methods), (ii) the lowest demonstrated detectable concentration, (iii) the test $H_{2(g)}$ concentration range, and (iv) response and recovery times such as onset time and t_{90}, explicitly stating the $H_{2(g)}$ concentration, temperature, and flow (or static) conditions used. Consistent reporting in vol% $H_{2(g)}$ (and when relevant, the corresponding dissolved H_2 concentration and conditions) would greatly improve comparability and allow clarity when identifying design principles to accelerate the rational development of next-generation optical $H_{2(g)}$ sensors.

Overall, dye-based $H_{2(g)}$ sensors show significant advantage over other $H_{2(g)}$ sensing modalities including non-dye based optical sensors. The continued investigation into these systems to develop better catalysts, dyes, and material designs will be essential for the progression of next-generation $H_{2(g)}$ sensors that meet the demands of safety monitoring, industrial use, and emerging $H_{2(g)}$-based technologies.

Author contributions

All authors contributed to the manuscript. All authors have given approval to the final version of the manuscript.

Conflicts of interest

The authors declare no competing financial interest.

Data availability

No primary research results, software or code have been included and no new data were generated or analysed as part of this review.

Acknowledgements

This work was partially funded by the Natural Sciences and Engineering Research Council of Canada (NSERC) through a Discovery Grant (RGPIN-2020-04480 to M. W. D. and RGPIN-2022-04428 to S. R. G.). M. P. thanks NSERC for financial support through a NSERC Postgraduate Scholarship – Doctoral.

References

1 A. M. Oliveira, R. R. Beswick and Y. Yan, *Curr. Opin. Chem. Eng.*, 2021, **33**, 100701.
2 A. Ishola, *World J. Adv. Res. Rev.*, 2024, **24**, 1373–1380.
3 M. J. B. Kabeyi and O. A. Olanrewaju, *Front. Energy Res.*, 2022, **9**, 743114.
4 K. T. Møller, T. R. Jensen, E. Akiba and H. Li, *Prog. Nat. Sci. Mater. Int.*, 2017, **27**, 34–40.
5 M. Ahad, M. Bhuiyan, A. Sakib, A. Becerril Corral and Z. Siddique, *Materials*, 2023, **16**, 6680.
6 I. Dincer and A. S. Joshi, in *Solar Based Hydrogen Production Systems*, Springer New York, New York, NY, 2013, pp. 1–5.
7 S. K. Menon, A. Kumar and S. Mondal, *Clean Energy*, 2025, **9**, 263–277.
8 International Energy Agency, *Global Hydrogen Review*, 2024.
9 International Energy Agency, *Global Hydrogen Review*, 2025.
10 T. Hübert, L. Boon-Brett, V. Palmisano and M. A. Bader, *Int. J. Hydrogen Energy*, 2014, **39**, 20474–20483.
11 W. J. Buttner, M. B. Post, R. Burgess and C. Rivkin, *Int. J. Hydrogen Energy*, 2011, **36**, 2462–2470.
12 T. Hübert, L. Boon-Brett, G. Black and U. Banach, *Sens. Actuators, B*, 2011, **157**, 329–352.
13 G. Korotcenkov, S. D. Han and J. R. Stetter, *Chem. Rev.*, 2009, **109**, 1402–1433.
14 E. Gorbova, G. Balkourani, C. Molochas, D. Sidiropoulos, A. Brouzgou, A. Demin and P. Tsiakaras, *Catalysts*, 2022, **12**, 1647.
15 M. Watanabe, R. Inoue, D. Ichikawa and K. Furusaki, *ECS Trans.*, 2010, **28**, 31–42.
16 Z. Zou, H. Zhang, Y. Sun, Y. Gao and L. Dou, *Rev. Sci. Instrum.*, 2022, **93**, 035001.
17 D. Berndt, J. Muggli, F. Wittwer, C. Langer, S. Heinrich, T. Knittel and R. Schreiner, *Sens. Actuators, A*, 2020, **305**, 111670.
18 E.-B. Lee, I.-S. Hwang, J.-H. Cha, H.-J. Lee, W.-B. Lee, J. J. Pak, J.-H. Lee and B.-K. Ju, *Sens. Actuators, B*, 2011, **153**, 392–397.
19 I. I. Ivanov, A. M. Baranov, V. A. Talipov, S. M. Mironov, S. Akbari, I. V. Kolesnik, E. D. Orlova and K. S. Napolskii, *Sens. Actuators, B*, 2021, **346**, 130515.
20 E. Brauns, E. Morsbach, S. Kunz, M. Bäumer and W. Lang, *Sens. Actuators, B*, 2014, **193**, 895–903.
21 S. Phanichphant, *Procedia Eng.*, 2014, **87**, 795–802.
22 Y. Luo, C. Zhang, B. Zheng, X. Geng and M. Debliquy, *Int. J. Hydrogen Energy*, 2017, **42**, 20386–20397.
23 C. Schultealbert, J. Amann, T. Baur and A. Schütze, *Atmosphere*, 2021, **12**, 366.
24 X. M. H. Huang, M. Manolidis, S. C. Jun and J. Hone, *Appl. Phys. Lett.*, 2005, **86**, 143104.
25 C. Wadell, S. Syrenova and C. Langhammer, *ACS Nano*, 2014, **8**, 11925–11940.
26 J. R. Stetter, W. R. Penrose and S. Yao, *J. Electrochem. Soc.*, 2003, **150**, S11.
27 A. S. Manna, S. Ghosh, T. Ghosh, N. Karchaudhuri, S. Das, A. Roy and D. K. Maiti, *Chem.–Asian J.*, 2025, **20**, e202401328.
28 M. Glass-Maujean and H. Schmoranzer, *J. Mol. Spectrosc.*, 2022, **385**, 111598.
29 M. Lin, *Can. J. Chem.*, 1966, **44**, 1237–1238.
30 D. D. Eley, in *Advances in Catalysis*, Elsevier, 1948, vol. 1, pp. 157–199.
31 I. Langmuir, *J. Am. Chem. Soc.*, 1912, **34**, 860–877.
32 D. R. Aireddy and K. Ding, *ACS Catal.*, 2022, **12**, 4707–4723.
33 S. J. B. Corrigan, *J. Chem. Phys.*, 1965, **43**, 4381–4386.
34 A. Melese, W. Wubet, A. Hussen, A. Temesgen and K. Mulate, *J. Chem. Res.*, 2025, **49**, 17475198251313648.
35 H. D. Kaesz and R. B. Saillant, *Chem. Rev.*, 1972, **72**, 231–281.
36 J. F. Hartwig, *Organotransition Metal Chemistry: from Bonding to Catalysis*, University Science Books, Sausalito, Calif, 2010.

37 G. J. Kubas, *Metal Dihydrogen and σ-Bond Complexes: Structure Theory and Reactivity*, Springer US, Boston, MA, 2001.
38 A. Roessler, O. Dossenbach, W. Marte and P. Rys, *Dyes Pigm.*, 2002, **54**, 141–146.
39 K. Chen, D. Yuan and Y. Zhao, *Opt. Laser Technol.*, 2021, **137**, 106808.
40 M. H. Yaacob, M. Breedon, K. Kalantar-zadeh and W. Wlodarski, *Sens. Actuators, B*, 2009, **137**, 115–120.
41 C. Gao, X. Guo, L. Nie, X. Wu, L. Peng and J. Chen, *Int. J. Hydrogen Energy*, 2023, **48**, 2442–2465.
42 A. K. Pathak, S. Verma, N. Sakda, C. Viphavakit, R. Chitaree and B. M. A. Rahman, *ACS Photonics*, 2023, **10**, 122.
43 P. Ngene, T. Radeva, M. Slaman, R. J. Westerwaal, H. Schreuders and B. Dam, *Adv. Funct. Mater.*, 2014, **24**, 2374–2382.
44 A. F. Girão and A. Completo, *Int. J. Hydrogen Energy*, 2024, **65**, 593–605.
45 X. She, Q. Yao, Q. Zou, G. Yang, Y. Shen and C. Jin, *ACS Appl. Mater. Interfaces*, 2023, **15**, 16244–16252.
46 X. She, Y. Shen, J. Wang and C. Jin, *Light Sci. Appl.*, 2019, **8**, 4.
47 X. She, Q. Yao, G. Yang, Y. Shen and C. Jin, *ACS Sens.*, 2022, **7**, 116–122.
48 Z. Chen, X. Wu, H. Liu, M. A. Baqir, K. Yu and K. Zhang, *Int. J. Hydrogen Energy*, 2024, **81**, 812–818.
49 Ö. Çoban, S. Tekmen, E. Gür and S. Tüzemen, *Int. J. Hydrogen Energy*, 2022, **47**, 25454–25464.
50 L. J. Bannenberg, F. A. A. Nugroho, H. Schreuders, B. Norder, T. T. Trinh, N.-J. Steinke, A. A. Van Well, C. Langhammer and B. Dam, *ACS Appl. Mater. Interfaces*, 2019, **11**, 15489–15497.
51 C. Chiu and M. H. Huang, *Angew. Chem., Int. Ed.*, 2013, **52**, 12709–12713.
52 M. Pasturel, M. Slaman, D. M. Borsa, H. Schreuders, B. Dam, R. Griessen, W. Lohstroh and A. Borgschulte, *Appl. Phys. Lett.*, 2006, **89**, 021913.
53 E. Herkert, F. Sterl, N. Strohfeldt, R. Walter and H. Giessen, *ACS Sens.*, 2020, **5**, 978–983.
54 M. E. Nasir, W. Dickson, G. A. Wurtz, W. P. Wardley and A. V. Zayats, *Adv. Mater.*, 2014, **26**, 3532–3537.
55 *Principles of Fluorescence Spectroscopy*, ed. J. R. Lakowicz, Springer US, Boston, MA, 2006, pp. 27–61.
56 *Introduction to Fluorescence Sensing*, ed. A. P. Demchenko, Springer Netherlands, Dordrecht, 2009, pp. 65–118.
57 Z. Jin, W. Yim, M. Retout, E. Housel, W. Zhong, J. Zhou, M. S. Strano and J. V. Jokerst, *Chem. Soc. Rev.*, 2024, **53**, 7681–7741.
58 S. A. Ali, M. Usman and M. N. Shaikh, *Small*, 2026, **22**, e11191.
59 S. Wintzheimer, T. Granath, M. Oppmann, T. Kister, T. Thai, T. Kraus, N. Vogel and K. Mandel, *ACS Nano*, 2018, **12**, 5093–5120.
60 K. Namba, S. Ogura, S. Ohno, W. Di, K. Kato, M. Wilde, I. Pletikosić, P. Pervan, M. Milun and K. Fukutani, *Proc. Natl. Acad. Sci. U. S. A.*, 2018, **115**, 7896–7900.
61 Y. Guo, J. Bae, Z. Fang, P. Li, F. Zhao and G. Yu, *Chem. Rev.*, 2020, **120**, 7642–7707.
62 Y. Wu, S. Joseph and N. R. Aluru, *J. Phys. Chem. B*, 2009, **113**, 3512–3520.
63 X. Huang and L. Zhang, *Chem. Eng. J.*, 2024, **484**, 149631.
64 Q. Wu, W. Xiong and G. Yang, *ChemCatChem*, 2025, **17**, e00902.
65 M. Falorni, G. Giacomelli, A. Porcheddu and M. Taddei, *J. Org. Chem.*, 1999, **64**, 8962–8964.
66 R. L. Courtney and L. A. Harrah, *J. Mater. Sci.*, 1977, **12**, 175–186.
67 E. A. Sangalang, H. N. Sharma, C. K. Saw, R. Gollott, S. M. Matt, T. S. Wilson, W. McLean, R. S. Maxwell and L. N. Dinh, *ACS Appl. Mater. Interfaces*, 2020, **12**, 3993–4001.
68 S. M. Matt, R. S. Maxwell, W. McLean and L. N. Dinh, *J. Phys. Chem. C*, 2022, **126**, 17712–17719.
69 Y. Luzzatto, A. Alatawna, G. Sror, O. Mendelson, S. Pevzner and O. Regev, *Int. J. Hydrogen Energy*, 2025, **137**, 397–405.
70 Y. Zhou, W. Wei, H. Su and W. Wang, *Inorg. Chem. Commun.*, 2019, **106**, 139–143.
71 L. N. Dinh, G. A. Cairns, R. A. Strickland, W. McLean and R. S. Maxwell, *J. Phys. Chem. A*, 2015, **119**, 943–951.
72 M. E. Smith, A. L. Stastny, J. A. Lynch, Z. Yu, P. Zhang and W. R. Heineman, *Anal. Chem.*, 2020, **92**, 10651–10658.
73 M. E. Smith, D. P. Rose, X. Cui, A. L. Stastny, P. Zhang and W. R. Heineman, *Anal. Chem.*, 2021, **93**, 10487–10494.
74 L. McDonnell, C. O'Rourke, M. Watson and A. Mills, *Analyst*, 2026, **151**, 1936–1947.
75 T. Seo, R. Kurokawa and B. Sato, *Med. Gas Res.*, 2012, **2**, 1.
76 S. Wintzheimer, J. Reichstein, P. Groppe, A. Wolf, B. Fett, H. Zhou, R. Pujales-Paradela, F. Miller, S. Müssig, S. Wenderoth and K. Mandel, *Adv. Funct. Mater.*, 2021, **31**, 2011089.
77 J. Reichstein, S. Schötz, M. Macht, S. Maisel, N. Stockinger, C. C. Collados, K. Schubert, D. Blaumeiser, S. Wintzheimer, A. Görling, M. Thommes, D. Zahn, J. Libuda, T. Bauer and K. Mandel, *Adv. Funct. Mater.*, 2022, **32**, 2112379.
78 K. Zhang, S. Schötz, J. Reichstein, P. Groppe, N. Stockinger, S. Wintzheimer, K. Mandel, J. Libuda and T. Retzer, *J. Chem. Phys.*, 2023, **158**, 134722.
79 K. Zhang, J. Reichstein, P. Groppe, S. Schoetz, N. Stockinger, J. Libuda, K. Mandel, S. Wintzheimer and T. Retzer, *Chem. Mater.*, 2023, **35**, 6808–6822.
80 J. Reichstein, P. Groppe, N. Stockinger, C. Cuadrado Collados, M. Thommes, S. Wintzheimer and K. Mandel, *Adv. Mater. Technol.*, 2024, **9**, 2400441.
81 A. Zink, J. Reichstein, N. Ruhland, N. Stockinger, B. S. Morozov, C. Cuadrado Collados, M. Thommes, E. A. Kataev, S. Wintzheimer and K. Mandel, *Chem. Commun.*, 2024, **60**, 5840–5843.
82 S. Wenderoth, M. Oppmann, D. Dzoic, T. Zimmermann, M. Lejoyeux, A. Graff, B. Schug and S. Wintzheimer, *Adv. Opt. Mater.*, 2026, e03568.
83 J. A. Osborn, F. H. Jardine, J. F. Young and G. Wilkinson, *J. Chem. Soc. A*, 1966, 1711.
84 A. F. Borowski, D. J. Cole-Hamilton and G. Wilkinson, *Chem. Informationsdienst*, 1978, **9**, chin.197826100.

85 T. Katsuda, H. Ooshima, M. Azuma and J. Kato, *J. Biosci. Bioeng.*, 2006, **102**, 220–226.
86 P. S. Schrader, E. H. Burrows and R. L. Ely, *Anal. Chem.*, 2008, **80**, 4014–4019.
87 P. Kos and H. Plenio, *Angew. Chem., Int. Ed.*, 2015, **54**, 13293–13296.
88 P. Kos and H. Plenio, *Chem.–Eur. J.*, 2015, **21**, 1088–1095.
89 A. Loudet and K. Burgess, *Chem. Rev.*, 2007, **107**, 4891–4932.
90 M. Potter, S. Debnath, P. Mandapati, K. Schmidt, K. Janzen, M. W. Drover, S. Rondeau-Gagné and B. Mutus, *ACS Sens.*, 2025, **10**, 2173–2180.
91 J. F. Hull, Y. Himeda, W.-H. Wang, B. Hashiguchi, R. Periana, D. J. Szalda, J. T. Muckerman and E. Fujita, *Nat. Chem.*, 2012, **4**, 383–388.
92 M. Potter, S. Debnath, M. W. Drover, S. Rondeau-Gagné and B. Mutus, *ACS Appl. Mater. Interfaces*, 2023, **15**, 43880–43886.
93 D. Fisher, M. Potter, P. Mandapati, M. W. Drover, S. Rondeau-Gagné and B. Mutus, *ACS Sustainable Chem. Eng.*, 2025, **13**, 15302–15310.
94 W. Liu, B. Sahoo, K. Junge and M. Beller, *Acc. Chem. Res.*, 2018, **51**, 1858–1869.
95 P. Wang, Z. He, Z. Xia, J. Wei and X. Dong, *Chin. J. Chem.*, 2024, **42**, 3135–3156.
96 D. Wei and C. Darcel, *Chem. Rev.*, 2019, **119**, 2550–2610.
97 J. Zhang, L. Tian, S. Shen, H. Zhang, L. Jia, X. Shi, W. Zhong, L. Zhang, C. Qiu and J. Wang, *Energy Mater.*, 2026, **6**, 600010.
98 Y.-Y. Li, S.-L. Yu, W.-Y. Shen and J.-X. Gao, *Acc. Chem. Res.*, 2015, **48**, 2587–2598.
99 S. Lentijo-Mozo, R. P. Tan, C. Garcia-Marcelot, T. Altantzis, P.-F. Fazzini, T. Hungria, B. Cormary, J. R. Gallagher, J. T. Miller, H. Martinez, S. Schrittwieser, J. Schotter, M. Respaud, S. Bals, G. V. Tendeloo, C. Gatel and K. Soulantica, *ACS Nano*, 2015, **9**, 2792–2804.
100 S. Fernández, S. Fernando and O. Planas, *Dalton Trans.*, 2023, **52**, 14259–14286.